PERGAMON International Journal of Multiphase Flow 24 (1998) 1057–1078

International Journal of Multiphase Flow

A novel centrifugal gas–liquid separator for catching intermittent flows

M. Creutz *, D. Mewes

Institute of Process Engineering, Hannover University, Callinstr. 36, 30167, Hannover, Germany

Received 30 December 1997; received in revised form 14 June 1998

Abstract

For separating transient two phase gas–liquid flows, a tool is developed that is based on a rotational pump impeller with axial gas removal. Theoretical and experimental investigations are presented concerning the transient behaviour of the separator and the quality of the separation. The basics of the hydrodynamic layout of the separator are presented for steady state and transient conditions. © 1998 Published by Elsevier Science Ltd. All rights reserved.

Keywords: Gas–liquid separator; Slug catcher; Intermittent flow; Dynamic modelling

1. Introduction

In various applications two phase gas–liquid flows have to be separated. For that purpose, static gravity separators are often used. For transient slug flow and high pressures at the separator inlet, these are large and costly tools (Hollenberg et al., 1995). For this reason intensive effort has been undertaken to develop separation techniques that use centrifugal forces in order to reduce their dimensions. Kouba et al. (1995) and Nebrensky et al. (1980) developed cyclone separators for the off-shore industry. Muschelknautz and Mayinger (1990) use rotating impellers for separating the liquid–gas mixture of a blowdown process in chemical reactors.

A new concept for transient gas–liquid separation is based on a rotary pump with gas-separation inside the impeller. The separator is shown schematically in Fig. 1. It consists of a stationary casing and a rotating shaft with an impeller. In contrast to the impeller of a centrifugal pump, this impeller is open on both sides. The liquid is forced through the impeller

* Corresponding author.

PII: S0301-9322(98)00018-4

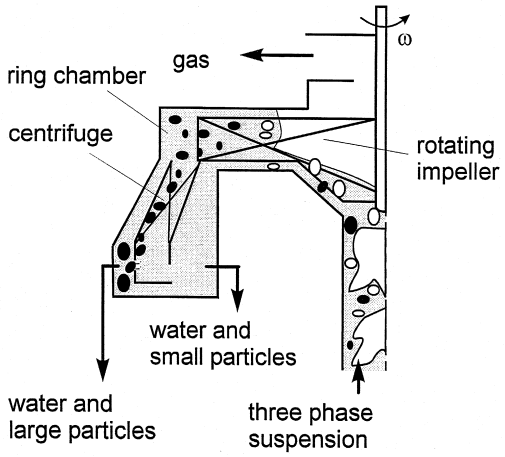

Fig. 1. Schematic of the separator.

into a ring chamber by means of centrifugal forces and the pressure is increased. The gas penetrates the impeller in the axial direction and leaves the separator. If the flow that enters the separator is intermittent, the liquid flow rate has to be damped in order to obtain a steady liquid outflow with low pressure fluctuations behind the impeller. The liquid flow fluctuations are moderated using a variable positioning of the interface between gas and liquid inside the impeller. A further separation of solid particles from the liquid is additionally obtained through a centrifuge mounted below the impeller. The solid–liquid separation is described by Creutz (1998) and not discussed in the current paper.

The two phase separator can be considered as a combination of a slug catcher, a separator and a pump in the process and in the off-shore industry. The three phase separator including the solid–liquid centrifuge is applied in underwater cutting processes where gaseous and solid contaminants are emitted, removed together with water and separated. These contaminants reduce the optic transparency of water. They have to be avoided in processes controlled by systems based on visual observation, especially in cutting processes used for the demolition of nuclear power plants. In the latter case, the contaminants have to be separated under extremely space-limited conditions.

The physical basics for the layout of the separator are deduced in the current paper for steady state and dynamic operating conditions. Experimental and theoretical investigations on the dynamic behaviour and on the quality of the gas separation are also presented.

2. Separator layout and experimental facility

The technical drawing of the separator manufactured from stainless steel is shown in Fig. 2. The inlet pressure and the back-pressure may vary between 0 and 11 bar, the pressure difference between outlet and inlet can be increased up to 5 bar. The rotor is driven by a 1.5 kW electric motor with speeds up to 50 rps. Several glass windows are mounted in the casing to enable visual observations and laser based flow measurements. The shaft is coupled to the

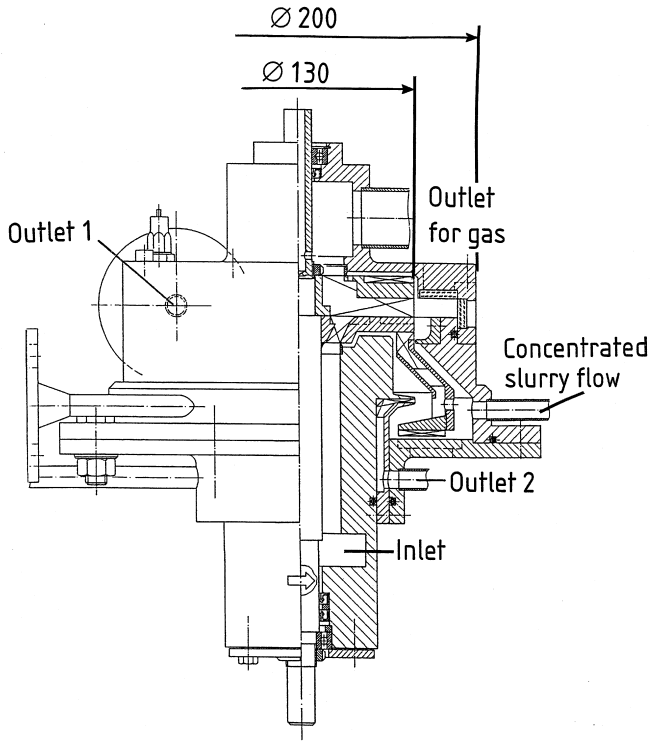

Fig. 2. Technical drawing of the separator.

motor on one side and the opposite side is manufactured as a hollow shaft which enables the electrical connection to a sensor that is placed inside the impeller. The impeller consists of eight blades, has a diameter of 130 mm and a clearance of 11 mm. The liquid flow enters the impeller in the axial direction and leaves it in the radial direction. The maximum gas flow rate is about 10 l/s, the maximum liquid flow rate depends on the backpressure and is 0.5 l/s for the present investigations. The separator shown in Fig. 2 acts also as a solid–liquid separator. The solid–liquid separation is carried out in a centrifuge mounted below the impeller. Solid particles are directed to the outer shell of the centrifuge by means of centrifugal forces and leave the separator continuously within a concentrated slurry flow. For the current investigations, only a two phase gas–liquid flow is considered. Investigations on three phase separation are reported on by Creutz (1998). Two outlets for the liquid are used as shown in Fig. 2. Outlet 1 is connected to the outer circumference of the impeller and resembles the typical configuration of a two-phase gas/liquid separator. Outlet 2 is the connection for the clean liquid leaving the centrifuge.

The experimental set up is shown in Fig. 3. The water-air two phase flow is fed into the separator via a 4 m long horizontal pipe (ID 16 mm). A transient slug flow is established in this pipe. The gas is separated and released to the atmosphere, the liquid leaves the separator either through outlet 1 or 2. The separated liquid may contain small amount of small gas bubbles. The mass flow and the mean density of the mixture is measured by a Coriolis

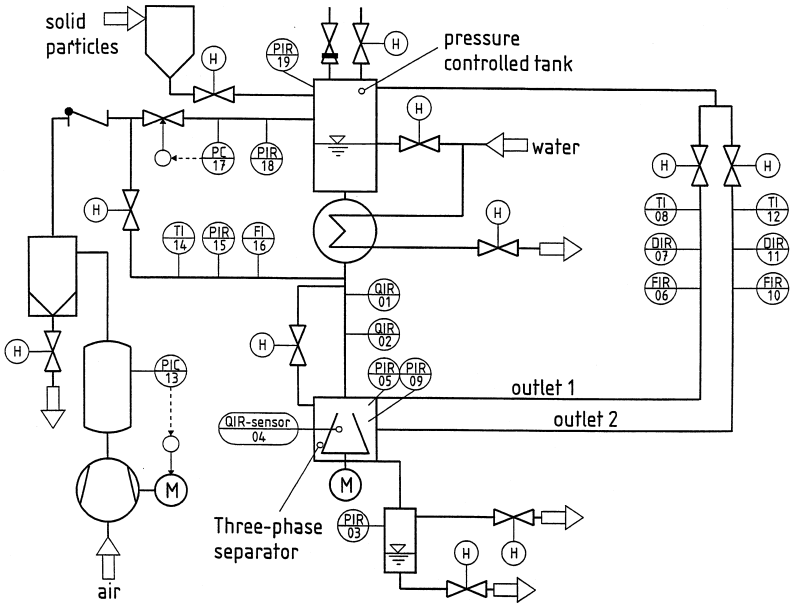

Fig. 3. Schematic of the experimental set up.

flowmeter. Assuming no slip, this allows for the determination of the individual mass flow rates of gas and liquid. The liquid flow is sent back into the storage vessel where remnants of gas in the flow are removed by gravity. The total pressure in the system is controlled by a valve connected to the gas outlet. The pressure is also controlled inside the storage tank. The liquid flow rate is controlled by the pressure difference between the storage tank and the separator that corresponds to the two-phase pressure drop in the supply pipe while the gas flow rate is adjusted by a hand valve. The back pressure to the separator is regulated by valves in each of the liquid lines. The system can be operated with three-phase gas/liquid/solid flow as well.

3. Measurement technique

The system used for the measurement of the time-dependent variables is shown in Fig. 4. The flow at the inlet of the separator is a slug flow. The mean volumetric liquid flow rate is measured by the Coriolis flowmeter at the outlet of the separator. The mean liquid fraction inside the cross section of the supply pipe is measured at two axially displaced positions via two pairs of ring electrodes with a frequency of up to 1 kHz. From these two measurements, the slug velocity of the two phase gas–liquid flow is calculated via a cross correlation between the two electrodes. From the liquid fraction, the slug velocity and the mean liquid flow rate, the dynamic liquid flow rate at the inlet of the separator is obtained (for details see Creutz, 1998). The back-pressure is measured by means of a pressure transducer. The liquid fraction

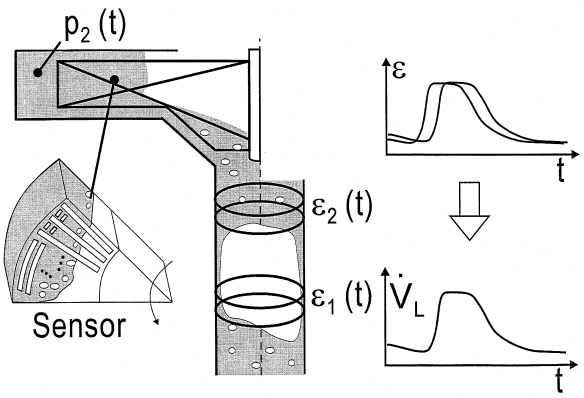

Fig. 4. Schematic of the positions for the time-dependent measurements.

inside the impeller is measured by means of an electrical resistance sensor as a function of the radial and the circumferential angle.

A schematic of the sensor and the electrodes is shown in Fig. 5. It is an integral part of the impeller and is located between two neighboring blades. Ten electrodes along the circumference and six electrodes along the radius of the impeller are used to measure an integral liquid fraction. The electrical potential of the counterpart of the electrode is grounded as well as all steel parts of the separator. The liquid fraction is a function of the electrical resistance between the electrode and the conducting counterpart of the sensor. The electrodes are surrounded by an electrical shield that provides a homogeneous electric field close to the electrodes leading to a linear relationship between liquid fraction and electrical resistance. Moreover, the electric shield damps the two-dimensional effects. The electrical potential in a radial cross section through the impeller resulting from a two dimensional finite-difference calculation is shown in Fig. 6. The highest current densities are obtained between the shield and the conducting

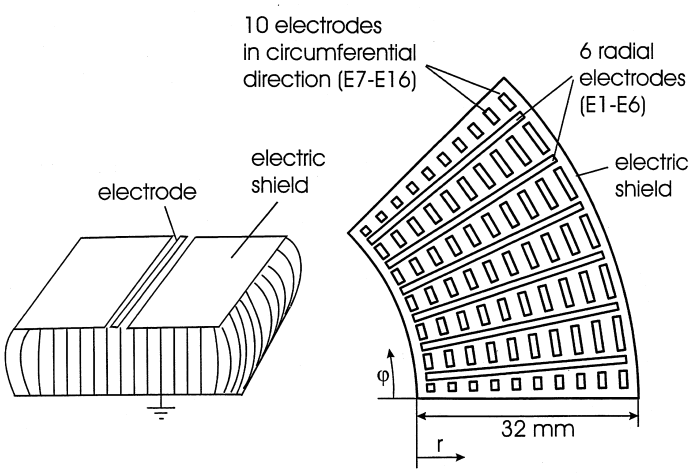

Fig. 5. Schematic of the sensor and the electrodes.

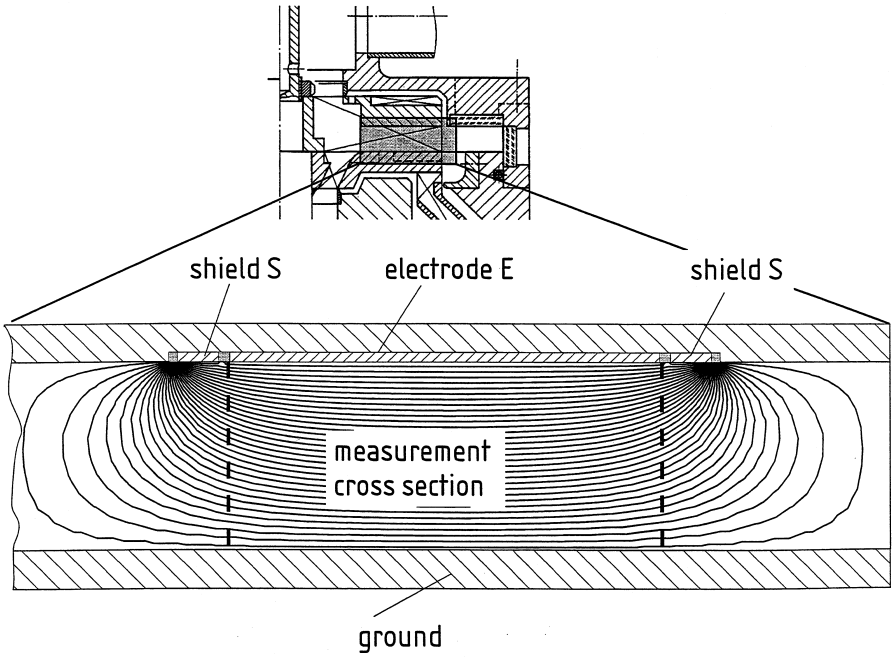

Fig. 6. Iso-potential lines for a radial cross section through the sensor.

material of the impeller. Here, the current density is approximately 10 times larger than inside the measurement cross section region, where the electrical field is nearly homogeneous.

The electronic data acquisition of the sensor is shown schematically in Fig. 7. The electrodes are multiplexed by Siliconix SMD-analog multiplexers with an inner resistance of about 40 Ω. A 4-Bit binary code (A0-A3) to control the multiplexers is provided by a PC. The selected electrode (E) and the counterpart of the sensor (M) that is set to the ground potential are connected to a 250 Ω Wheatstone bridge. The bridge is supplied by 1.5 V AC voltage with a frequency of 5 kHz. The signal of the bridge is amplified by a frequency shift amplifier, converted into a 12 bit digital signal and stored in the PC. The measurement frequency for a single electrode is 1 kHz and for a complete set of 16 electrodes it is 62.5 Hz. The electric shield is supplied with the alternating electrode potential, decoupled from the bridge by an operational amplifier. The multiplexers and the operational amplifier are embedded in the sensor and thus rotating with the impeller. The sensor is connected to a rotating measurement casing by cables through a drill-hole inside the shaft. High speed slip rings with an outer diameter of 0.8 mm are used for the electrical connection to the stationary parts of the data acquisition system. The metal structures of the separator are connected to the ground potential. The sensor is used for two different purposes. By using only one electrode in the radial direction, the position of the gas–liquid interface, h^* is measured with up to 1 kHz assuming a sharp interface. In combination with the back-pressure of the separator and the liquid flow rate, insight into the dynamic behavior of the system is obtained. These measurements are compared to a non-linear calculation in the following chapter. By using all electrodes, integral information on the liquid fraction inside the separator is obtained.

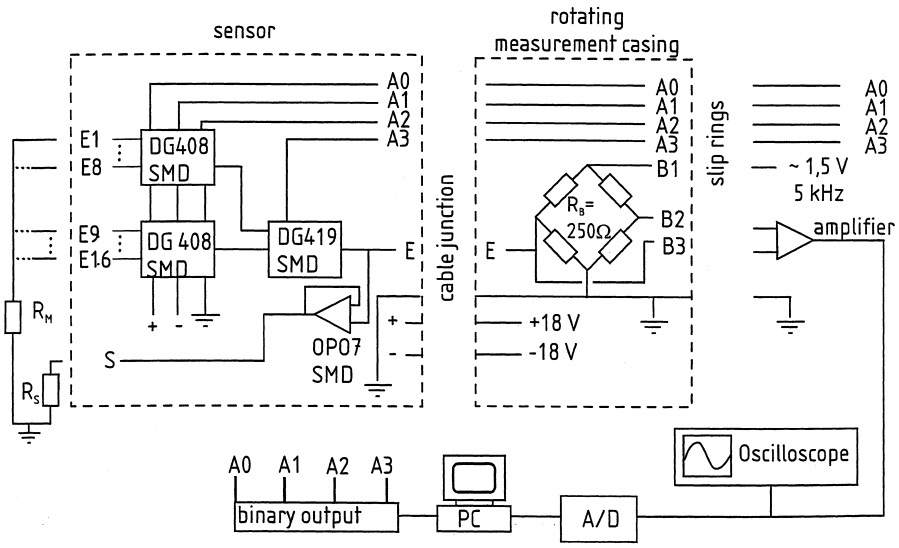

Fig. 7. Data acquisition system of the sensor.

4. Dynamic behavior of the separator and scale up

The dynamic behavior of the gas–liquid separation inside the impeller is quantified with a theoretical approach. The formulation enables the calculation of three unknown variables, i.e. the back pressure of the separator, the liquid flow rate that leaves the separator and the position of the gas–liquid interface as functions of the liquid flow rate that enters the separator. A schematic of the gas–liquid separation and the relevant geometric quantities are shown in Fig. 8. The subscripts 1 and 2 indicate the separator inlet and outlet, respectively and the subscript 0 stands for ambient conditions. The following assumptions are made in the analysis:

- The friction inside the impeller is negligible.
- The position of the interface is one-dimensional.

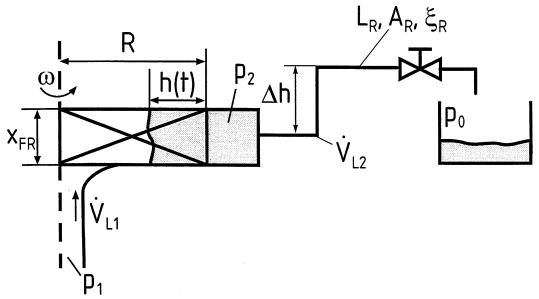

Fig. 8. Schematic of the impeller and the relevant geometric quantities.

- The liquid is completely removed from the gas and vice versa.
- The radial velocity of the liquid inside the impeller is approximately two orders lower than the tangential velocity and thus is neglected in the momentum equation.
- The angular velocity of the impeller is constant.
- Pressure drop due to acceleration is considered only in the outlet pipe.
- All balance equations are formulated in one dimension.

The three equations that are required for the mathematical solution are the mass and the momentum balance of the flow inside the impeller, and that for determining the pressure drop in the liquid outline. The mass balance of the flow through the impeller leads

$$\dot{V}_{\mathrm{L1}} - \dot{V}_{\mathrm{L2}} = \frac{\mathrm{d}V_{\mathrm{L,FR}}}{\mathrm{d}t} = (R-h)2\pi x_{\mathrm{FR}} \frac{\mathrm{d}h}{\mathrm{d}t}. \tag{1}$$

In this equation, $\dot{V}_{\mathrm{L1}}$ is the volumetric liquid flow rate entering the separator, $\dot{V}_{\mathrm{L2}}$ is the volumetric liquid flow rate that leaves the separator, R is the outer radius of the impeller, $V_{\mathrm{L,FR}}$ is the volume of liquid inside the impeller, h is the position of the interface, x_{FR} is the clearance of the impeller and t is the time. Following the above assumptions, the integral form of the momentum equation inside the impeller in the radial direction yields

$$p_2 - p_1 = \rho_{\mathrm{L}} \int_{R-h}^{R} \frac{v_{\mathrm{U}}^2}{r} \mathrm{d}r = \rho_{\mathrm{L}} \int_{R-h}^{R} \omega^2 r \, \mathrm{d}r = \frac{\rho_{\mathrm{L}}}{2} \omega^2 (2Rh - h^2) \tag{2}$$

with the pressure in the supply pipe, p_1 , the pressure behind the impeller, p_2, the density of the liquid, ρ_{L}, and the tangential velocity, v_{U} as a product of the radius r and the angular velocity ω. By the momentum equation, the position of the interface is dynamically correlated to the back pressure of the separator. The position of the interface adapts itself to a given pressure difference, (p_2-p_1) and, thus, inherently controls the system. For instance, by increasing the liquid flow rate entering the separator, the liquid level is increased. This leads to an increase of the outlet pressure and, thus, to an increase in the flow rate inside the following pipe. The liquid level adapts itself rapidly to variations in the liquid flow rate and allows for separating intermittent flows such as slug and plug flows. Friction, acceleration of the liquid and hydrostatic pressure drop are taken into account for calculating the pressure difference along the pipe:

$$p_2 - p_0 = \frac{\rho_{\mathrm{L}}}{2} \frac{\dot{V}_{\mathrm{L2}}^2}{R^4} \xi_{\mathrm{R}} + \rho_{\mathrm{L}} \sum_i \frac{L_{\mathrm{R},i}}{A_{\mathrm{R},i}} \frac{\partial \dot{V}_{\mathrm{L2}}^2}{\partial t} + \rho_{\mathrm{L}} f \Delta h. \tag{3}$$

In this equation, p_0 is the ambient pressure, the pipe is characterized by the sum of i sectional relationships of length, $L_{\mathrm{R},i}$ and cross sectional area, $A_{\mathrm{R},i}$ as well as by its static height Δh. The friction factor of the pipe is defined as

$$\xi_{\mathrm{R}} = \frac{\Delta p_{\mathrm{Reib}}}{\rho_{\mathrm{L/2}} \dot{V}_{\mathrm{L2}}^2} R^4. \tag{4}$$

The friction factor is obtained from experiments as a function of the liquid flow rate. Changing the friction factor by throttling the pipe, changes the mean position of the interface. High

amounts of the acceleration force result in high peaks of the backpressure of the separator and shrinks the possible range of operation. The system of equations (Eqs. (1)–(3)) can be written in dimensionless form

$$\dot{V}^*_{\mathrm{L1}} - \dot{V}^*_{\mathrm{L2}} = (1 - h^*)\frac{\partial h^*}{\partial Fo}, \tag{5}$$

$$Eu_2 - Eu_1 = \frac{1}{R^2}\int_{R-h}^{R} r \, \mathrm{d}r = 2h^* - h^{*2}, \tag{6}$$

and

$$Eu_2 - Eu_0 = \xi_{\mathrm{R}}\dot{V}^{*2}_{\mathrm{L2}} + D^*_{\mathrm{R}}\frac{\partial \dot{V}^*_{\mathrm{L2}}}{\partial Fo} + H^*, \tag{7}$$

with the dimensionless position of the interface

$$h^* = \frac{h}{R}, \tag{8}$$

the Fourier-number

$$Fo = \frac{t\omega R}{2\pi x_{\mathrm{FR}}}, \tag{9}$$

the dimensionless volumetric flow rate

$$\dot{V}^* = \frac{\dot{V}}{\omega R^3}, \tag{10}$$

the dimensionless hydrostatic pressure

$$H^* = \frac{2g\Delta h}{\omega^2 R^2}, \tag{11}$$

the Euler-number

$$Eu = \frac{2p}{\rho_{\mathrm{L}}\omega^2 R^2} \tag{12}$$

and the differential coefficient

$$D^*_{\mathrm{R}} = \frac{R^2}{\pi x_{\mathrm{FR}}}\sum_i \frac{L_{\mathrm{R},i}}{A_{\mathrm{R},i}}. \tag{13}$$

The above system of equations is non linear and is solved numerically by a modified Runge–Kutta method. The results of these calculations will be compared to measurements in the following section. For the steady state layout of the separator and for determining the operating conditions, the position of the interface is calculated as a function of volumetric flow rate, the backpressure and the angular velocity of the separator. For that purpose, neglecting

all derivatives to Fo yields the steady state solution of the system of equations

$$h^*_{\mathrm{stat}} = 1 - \sqrt{1 - (\xi_{\mathrm{R}} \dot{V}^{*2}_{\mathrm{stat}} + H^*)} = 1 - \sqrt{1 - Eu_{stat}} \tag{14}$$

with the steady state Euler-number

$$Eu_{\mathrm{stat}} \equiv Eu_2 - Eu_1 = Eu_2 - Eu_0. \tag{15}$$

from

$$Eu_{\mathrm{stat}} = \xi_{\mathrm{R}} \dot{V}^{*2}_{\mathrm{stat}} + H^*. \tag{16}$$

By linearizing Eqs. (5)–(7) around a steady state solution, a stability analysis is carried out. The linearization leads to

$$\begin{aligned} \dot{V}^+_{\mathrm{L1}} &= \dot{V}^+_{\mathrm{L2}} + T_1 \frac{\partial \dot{V}^+_{\mathrm{L2}}}{\partial Fo} + T_2^2 \frac{\partial^2 \dot{V}^+_{\mathrm{L2}}}{\partial Fo^2} \\ K_1\left(\dot{V}^+_{\mathrm{L1}} + T_{\mathrm{D}} \frac{\partial \dot{V}^+_{\mathrm{L1}}}{\partial t}\right) &= Eu_2^+ + T_1 \frac{\partial Eu_2^+}{\partial Fo} + T_2^2 \frac{\partial^2 Eu_2^+}{\partial Fo^2}\} \\ K_2\left(\dot{V}^+_{\mathrm{L1}} + T_{\mathrm{D}} \frac{\partial \dot{V}^+_{\mathrm{L1}}}{\partial t}\right) &= h^+ + T_1 \frac{\partial h^+}{\partial Fo} + T_2^2 \frac{\partial^2 h^+}{\partial Fo^2} \end{aligned} \tag{17}$$

with the linearized quantities that are indicated by ' + ' and defined in Appendix A1. The system output ($\dot{V}_{\mathrm{L2}}$, p_2 and h) can be calculated independent of each other for a given excitation of the system ($\dot{V}_{\mathrm{L1}}$). The pressure at the entrance of the separator, p_1 and the ambient pressure, p_0 are set equal as they are in the experimental investigations. The differential Eqs. (17) are of second order with the time constants T_1 and T_2. The differential part in the equations for the Euler-number and the position of the interface are indicated by the time constant T_{D}. The linearized system is stable. The damping coefficient of the linearized system is

$$D_{\mathrm{dyn}} \equiv \frac{T_1}{2T_2} = \frac{Eu_{\mathrm{stat}} - H^*}{\dot{V}^*_{\mathrm{stat}} \sqrt{2D^*_{\mathrm{R}}}} = \frac{p_{2\mathrm{stat}}}{\rho_{\mathrm{L}} \omega \dot{V}_{\mathrm{Lstat}}} \sqrt{\frac{\pi x_{\mathrm{FR}}}{2 \sum_i L_{\mathrm{R},i}/A_{\mathrm{R},i}}}. \tag{18}$$

High values of the damping coefficient lead to smoothing large variations of the volumetric liquid flow rate. Technically, the damping coefficient is enlarged by small angular velocities, by wide impeller clearances, by a high ratio of backpressure to volumetric flow rate and by short pipes connected to the impeller. A long pipe additionally leads to increasing the differential coefficient T_{D} and thus to increasing pressure peaks following each slug that enters the separator.

5. Experimental results

The plot of the reduced steady state Euler-number versus the dimensionless liquid flow rate is shown in Fig. 9. The theoretical prediction according to Eq. (16) is plotted as a line. The

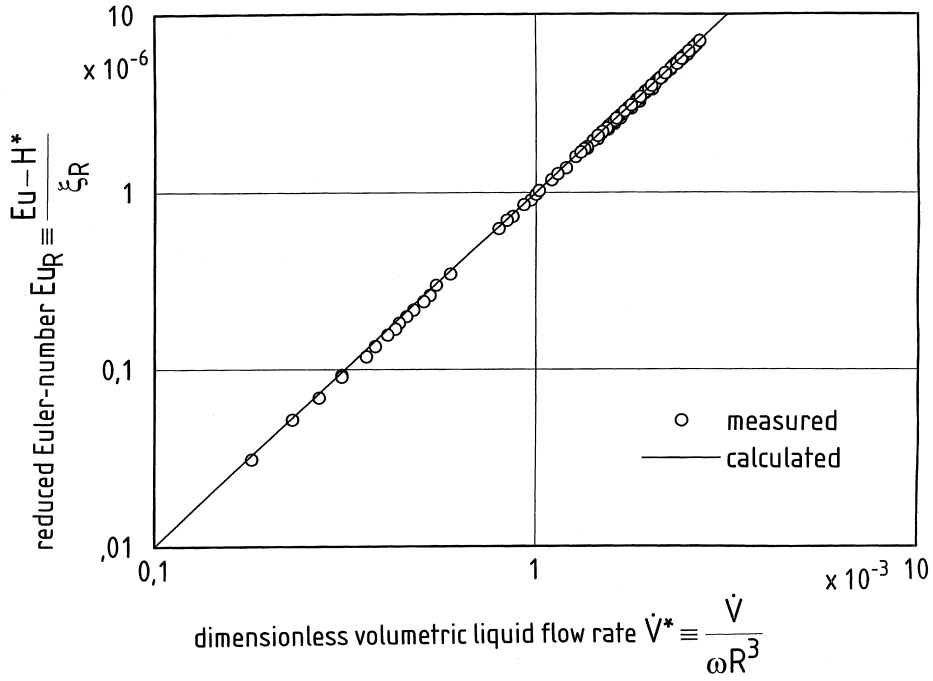

Fig. 9. Reduced steady state Euler-number as a function of the dimensionless liquid flow rate.

measurements are indicated as circles. They are based on variations of the separator's angular velocity, the volumetric flow rates of gas and liquid and on different kinds of liquid outlet pipes. The measurements resemble the theoretical prediction according to Eq. (12) with relative error of 5%. The reduced steady state Euler-number increases with the volumetric liquid flow rate to the power of two due to the turbulent flow in the liquid outlet pipe. This behavior elucidates the difference between the separator and a conventional centrifugal pump, where the back pressure usually decreases with increasing flow rate.

In Fig. 10, the position of the interface obtained from experimental investigations is shown as a function of the Euler-number and is compared with theoretical findings for steady state flow (Eq. (14)). The position of the interface moves to the inside of the impeller with increasing Euler-number. Due to the sensor geometry, the position can be measured between $0.03 < h^* < 0.54$. This region correlates with the Euler-numbers $0.06 < Eu < 0.79$. The measurements represented in the figure are obtained for liquid flow rates from 0.01 to 0.16 l/s and rotation frequencies between 8.5 and 50 Hz. The relative error of the measurements compared with Eq. (14) is $\pm 20\%$. This high value is due to the assumption of an ideal interface. In reality the interface consists of a foamy zone between gas and liquid bulk phase as will be shown later.

In the upper diagrams of Fig. 11 the pressure at the outlet of the separator is plotted as a function of time for an intermittent flow at the inlet. The liquid flow rate at the inlet and at the outlet of the separator is plotted in the lower diagrams. The inlet flow rate is measured and the outlet flow rate is obtained by the calculations. The inlet pipe has an inner diameter of 16 mm

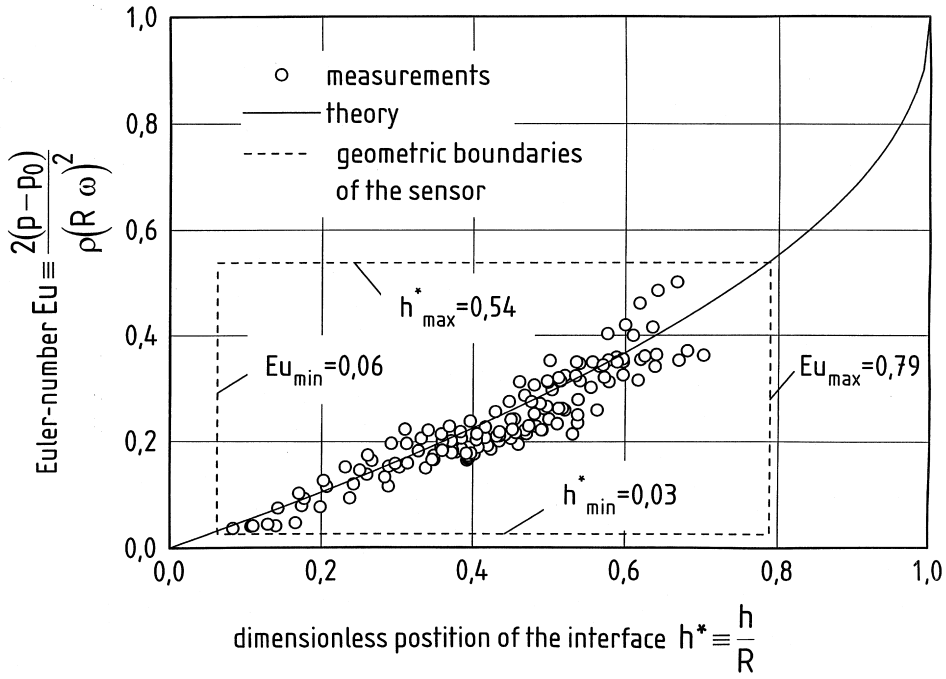

Fig. 10. Dimensionless position of the interface as a function of the Euler-number.

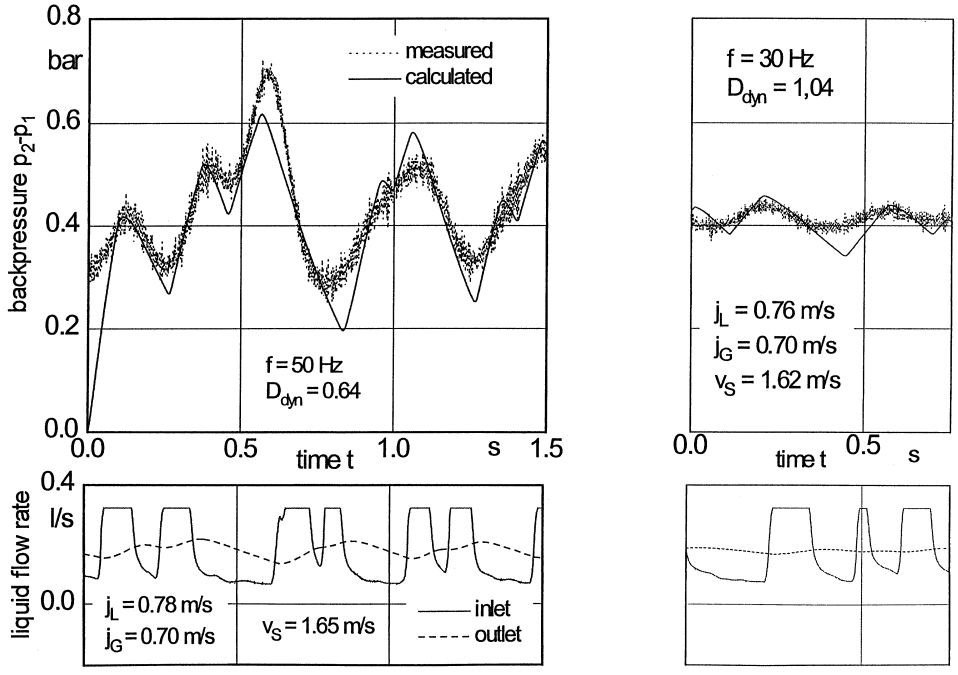

Fig. 11. Pressure and the volumetric liquid flow rate as functions of the time for different damping coefficients.

and is mounted horizontally. Slug and plug flow exists with high time variations of the liquid flow rate. The mean flow rates of gas and liquid at the inlet to the pipe are kept constant. The damping coefficient is varied by changing the separator frequency. For a damping coefficient of 0.64 (left diagrams) the pressure reacts strongly on variations in the flow rate. By increasing the damping coefficient to 1.04 (right diagrams) the back pressure of the separator as well as the flow rate in the outlet are more even. The fluctuations in the outlet flow rate are much smaller that the fluctuations in the back pressure due to the missing differential part in the corresponding equation (Eq. (17)). They also decrease with increasing damping coefficient. This fact could also be observed visually at the reflux to the storage tank. Technically, the damping coefficient should be maximized when separating intermittent flows to minimize pressure fluctuations and transient liquid outflows.

By solving the system of non-linear differential equations (Eqs. (1)–(3)) with the measured liquid flow rate at the inlet as a boundary condition, the back pressure p_2 and the outlet liquid flow rate are calculated. The calculated values of the pressure match the experimentally obtained ones. Since back pressure and outlet liquid flow rate are coupled by a well known physically based equation (Eq. (3)), the behaviour of the outlet liquid flow seems to be reasonable, although the values are not experimentally verified. The physical basics deducted from the experiments are accounted for in the theoretical approach.

6. Gas–liquid separation

Gas is pulled into the liquid by the radial impulse of the liquid impinging into the interface. Some little amount of the gas penetrates through the liquid and leaves the impeller together with the liquid flow. Experimental investigations have been carried out on the gas–liquid separation inside the impeller. The volumetric gas fraction inside the ring chamber at the outer circumference of the impeller has been measured by removing the liquid directly behind the impeller (outlet 1, see Fig. 2). The volumetric gas fraction of the flow inside the centrifuge has been measured by removing the liquid through outlet 2. The gas fraction of the liquid flow is shown as a function of the position of the interface in Fig. 12 using the two different outlets. The rotational velocity of the separator, the pressure drop in the pipeline behind the separator and the liquid flow rate are varied. The gas fraction decreases with increasing position of the interface because gas bubbles have to penetrate through a wider liquid ring inside the impeller. The gas fraction is decreased significantly between the ring chamber and the centrifuge. At the inlet to the centrifuge, the flow is set to a solid body rotation. Fluctuations are damped and gas bubbles are separated and are removed together with a small amount of liquid through a gap between impeller and solid casing and penetrate back into the flow that enters the separator. If the position of the interface exceeds the radial position of the gas outlet ($h^* = 0.58$), liquid is carried through the gas outlet. Under common operation conditions, no liquid-carryover could be observed visually. In a technical application the position of the interface is varied by changing the rotational velocity of the impeller or by throttling the liquid pipe. If the entering flow is steady, the liquid level should be close to the maximum value. In case of an intermittent inlet flow, the level should be set to a value below the maximum to enable variations of the interface without liquid-carryover. Generally, no centrifuge is needed

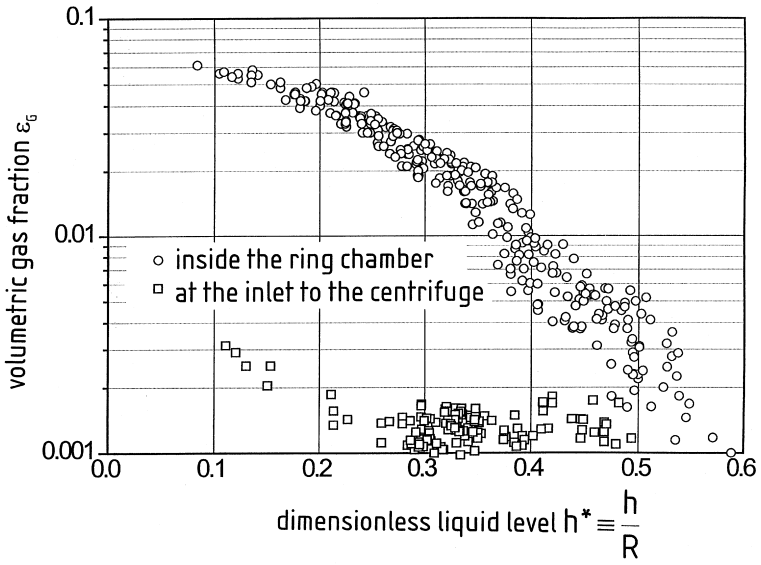

Fig. 12. Volumetric gas flow rate in the liquid outlet as a function of the position of the interface.

for gas–liquid separation. For this reason the following analysis concentrates on the flow inside the impeller only.

In Fig. 13, plot of the liquid fraction and the velocity field in an axial cross section through the impeller is shown as a result of a numerical 3-D Euler–Euler calculation of the two-phase flow. The numerical calculations are based on a four field model, i.e. gas and liquid are assumed to be present in both dispersed fields (bubbles and droplets) and in the continuous fields. For the present calculations, the centrifugal forces, the buoyancy and the impulse forces (including added mass) play dominant roles and overcome the drag effects. Thus, the dependence of the solution on the bubble and droplet sizes, that are kept constant, is only little. The method is described by Creutz (1998) in detail. It is visible that the interface is not sharp but a foamy region extending approximately 1 cm. The flow field is three-dimensional but the position of the interface varies little with the circumferential angle.

In Fig. 14 the mean liquid fraction that is integrated across the height and the circumference of the impeller is plotted as a function of the radius. The solution of the numerical calculation as well as experimental findings are shown. Experiments and calculations fit reasonable well except for a minimum liquid fraction in the continuous liquid region. This minimum characteristically occurs in all measurements and is explained by the trajectories of the bubbles through the liquid inside the impeller. The bubbles are initiated by the impingement of water on the gas–liquid interface with an initial velocity in the radial direction. The bubbles are decelerated, most bubbles stop and move back to the interface. The minimum liquid fractions indicates the position of low bubble velocity corresponding to the point of return of the majority of the bubbles.

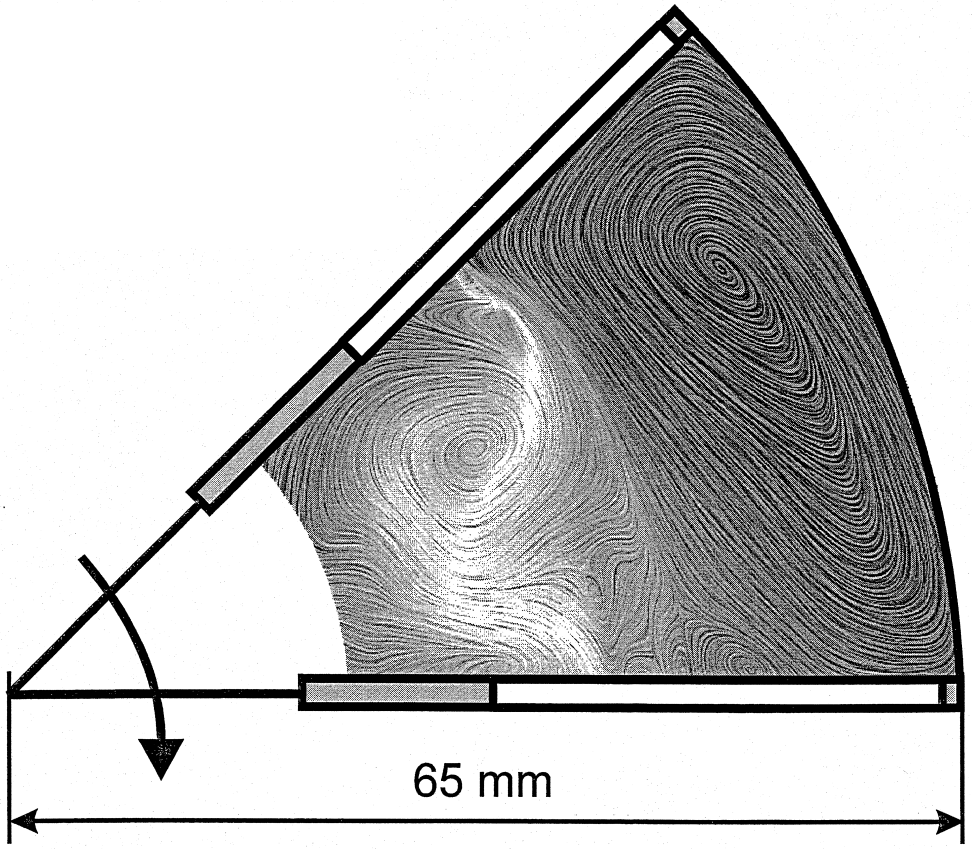

Fig. 13. Liquid fraction and the velocity field in an axial cross section through the impeller of the separator.

A semi-empirical one-dimensional steady state model is proposed to predict the volumetric gas flow rate that leaves the separator through the liquid outlet. A plot of energy fluxes in the impeller is given in Fig. 15. The continuous gas and liquid regions are divided by the interface. Energy fluxes in the radial direction that are transported by the dispersed droplets and bubbles are shown schematically. The liquid droplets are accelerated due to centrifugal forces before reaching the interface. Their kinetic energy flux of the liquid in radial direction at the interface is:

$$\dot{E}_{\mathrm{L}} = \frac{\rho_{\mathrm{L}}}{2} \dot{V}_{\mathrm{L}} \{v_{\mathrm{L,R}}(h)\}^2. \tag{19}$$

In this equation, $\dot{V}_{\mathrm{L}}$ is the volumetric liquid flow rate and $v_{\mathrm{L,R}}(h)$ is the velocity of the liquid reaching the interface. The energy flux is transferred from the liquid to the gas-bubbles (including added mass) through the interface. The bubbles are decelerated by the centrifugal body force and the drag force. Depending on their terminal velocity, they pass the impeller (gas energy flux $\dot{E}_{\mathrm{G1}}$) or they return to the interface and completely dissipate the gas energy

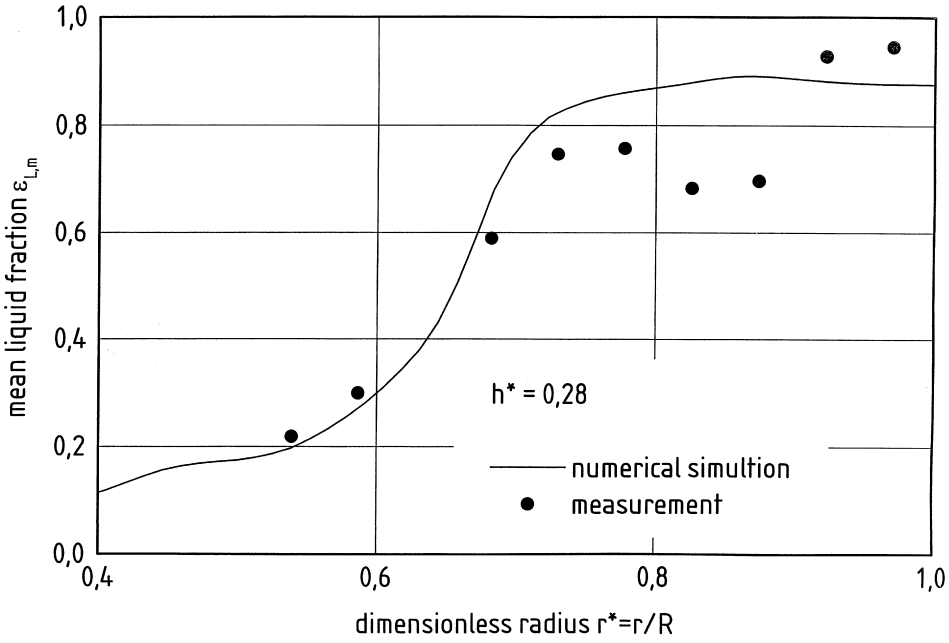

Fig. 14. Mean liquid fraction across the height and the circumference of the impeller as a function of the radius.

flux $\dot{E}_{G2}$. The total terminal energy flux of the gas equals the energy flux of the liquid at the interface ($\dot{E}_L = \dot{E}_{G1} + \dot{E}_{G2}$). The ratio of the gas energy flux $\dot{E}_{G1}$ to the energy flux of the liquid is calculated by the energy flux ratio

$$X_E \equiv \frac{\dot{E}_{G,1}}{\dot{E}_L}. \tag{20}$$

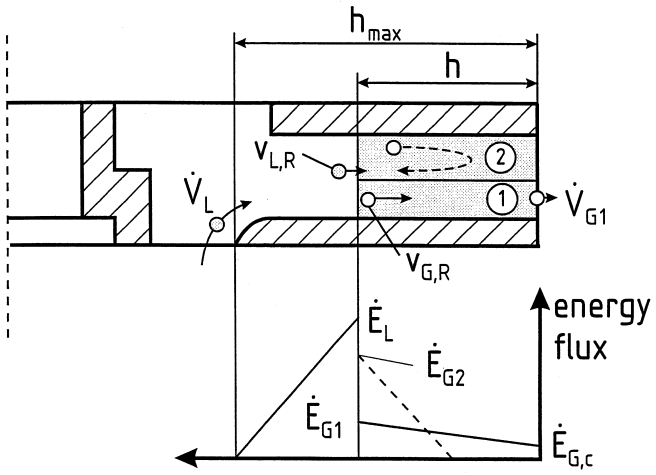

Fig. 15. Schematic of the multiphase flow and the energy fluxes inside the impeller.

The energy flux of the gas passing through the impeller is calculated by the kinetic energy of the gas bubbles leaving the interface:

$$\dot{E}_{G,1} = \frac{(\alpha\rho_L + \rho_G)}{2} \dot{V}_{G,1}\{v_{G,R}(h)\}^2 \tag{21}$$

In this equation, $\dot{V}_{G,1}$ is the volumetric liquid flow rate passing through the impeller, $v_{G,R}(h)$ is the radial terminal velocity of the corresponding gas bubbles at the interface and α is the added mass coefficient ($\alpha = 0.5$). The volumetric gas flow rate $\dot{V}_{G,1}$ is given by:

$$\dot{V}_{G,1} = X_E \dot{V}_L \frac{1}{\alpha + \frac{\rho_G}{\rho_L}} \left\{\frac{v_{L,R}(h)}{v_{G,R}(h)}\right\}^2 \tag{22}$$

or alternatively the gas fraction in the liquid outlet is given by:

$$\dot{\varepsilon} \equiv \frac{\dot{V}_{G,1}}{\dot{V}_{G,1} + \dot{V}_L} = \left\{1 + \frac{\alpha + \frac{\rho_G}{\rho_L}}{X_E}\left[\frac{v_{L,R}(h)}{v_{G,R}(h)}\right]^2\right\}^{-1}. \tag{23}$$

In these equations, the velocities of gas and liquid at the interface as well as the energy flux ratio are unknown. The latter one is assumed to depend on the layout of the impeller and its inlet only and will be obtained from experimental findings as an empirical constant. The velocities of the liquid at the interface is calculated assuming a constant centrifugal acceleration by integrating the momentum equation from the outer radius of the inlet to the position of the interface neglecting all frictional effects:

$$v_{L,R}(h) = (R\omega)\sqrt{(h^*_{max} - h^*)\left(1 - \frac{h^*_{max} + h^*}{2}\right)}. \tag{24}$$

In this equation, $h^*_{max} = 0.58$ is the position of the outer radius of the inlet. The derivation of the above equation is described in Appendix A2. The terminal velocity of the gas bubbles necessary for passing through the impeller is obtained from ist momentum equation in the radial direction:

$$F_T = F_F + F_Z. \tag{25}$$

In this equation, F_T is the inertia force, F_F is the friction force and F_Z is the body force due to the centrifugal acceleration. The inertia force is

$$F_T = \frac{\pi}{6} d_B^3 (\alpha\rho_L + \rho_G)\frac{d^2 r}{dt^2}, \tag{26}$$

the friction force is

$$F_F = -\frac{\pi}{4} d_B^2 \xi_B \left(\frac{dr}{dt}\right)\left|\frac{dr}{dt}\right| \text{ with the friction factor } \xi_B = \frac{24}{Re} = \frac{24 v_L}{\left|\frac{dr}{dr}\right| d_B} \tag{27}$$

for the Reynolds-number $Re < 1$. The centrifugal force is

$$F_T = \frac{\pi}{6} d_B^3 (\rho_G = \rho_L) r\omega^2. \tag{28}$$

In the above equations, d_B is the diameter of the bubble, r is the radius, t the time and v_L the kinematic viscosity of the liquid phase. Substituting eqns (26)–(28) in eqn (25) leads to the differential equation to calculate the position of the bubble as a function of time:

$$\frac{d^2 r}{dt^2} + C_A \frac{dr}{dt} + C_B r = 0$$

with

$$C_A \equiv 18 \frac{v_L}{d_B^2(\rho_G/\rho_L + \alpha)} \tag{29}$$

and

$$C_B \equiv \frac{\rho_L - \rho_G}{\alpha\rho_L + \rho_G}\omega^2.$$

That is solved to yield

$$r(t) = \frac{1}{e^{C_A t/2}} \left\{ \left(\frac{2v_0 + C_A r_0}{\omega_0} \right) \sin(\omega_0 t/2) + r_0 \cos(\omega_0 t/2) \right\} \tag{30}$$

with

$$\omega_0 \equiv \sqrt{4C_B - C_A^2} \quad \forall \quad 4C_B \geq C_A^2.$$

In this equation, v_0 is the terminal velocity of the gas bubble at the interface and $r_0 = R - h$ is the radial position of the interface. From this equation, the minimum terminal velocity $v_{0,\min}$ is calculated that enables the bubble to pass through the impeller. For that purpose, the boundary conditions

$$\left.\frac{dr}{dt}\right|_{t=t_w} = 0 \quad \text{and} \quad r(t = t_w) = R \tag{31}$$

have to be satisfied. In these equations, t_w is the time the bubble needs to reach the outer circumference of the impeller. From the boundary conditions, the following equations are obtained:

$$2v_{0,\min} = \frac{C_A(2v_{0,\min} + C_A r_0) + \omega_0^2 r_0}{2v_{0,\min}\omega_0} \tan(\omega_0 t_w/2). \tag{32}$$

$$R = \frac{\left(\frac{2v_{0,\min} + C_A r_0}{\omega_0} \right) \sin(\omega_0 t_w/2) + r_0 \cos(\omega_0 t_w/2)}{e^{C_A t_w/2}}. \tag{33}$$

From these equations, the time t_w and the velocity $v_{0,\min}$ are calculated. In dimensionless form, the minimum terminal velocity is defined as

$$v^*_{0,\min} \equiv \frac{v_{0,\min}}{v_{0,gr}} \equiv \frac{v_{0,\min}}{\omega\sqrt{2(R^2 - r_0^2)}}. \tag{34}$$

The dimensionless minimum terminal bubble velocity does not depend on the rotational velocity of the impeller. The bubble diameter is related to a characteristic bubble diameter

$$d^*_{B1} \equiv \frac{d_{B1}}{d_{B1,c}} \equiv \frac{d_{B1}}{3\sqrt{\frac{\nu_L}{\omega}}}\left\{\left(1 - \frac{\rho_G}{\rho_L}\right)\left(\frac{\rho_G}{\rho_L} + \alpha\right)\right\}^{1/4}. \tag{35}$$

The dimensionless minimum terminal bubble velocity is plotted vs the dimensionless bubble diameter in Fig. 16. With increasing diameter, the influence of the friction diminishes, the minimum velocity remains constant. Here, the analysis becomes independent of the bubble diameter. Smaller gas bubbles tend to return to the interface and are accounted for by the energy flux ratio. It is assumed that the diameter of all gas bubbles passing through the

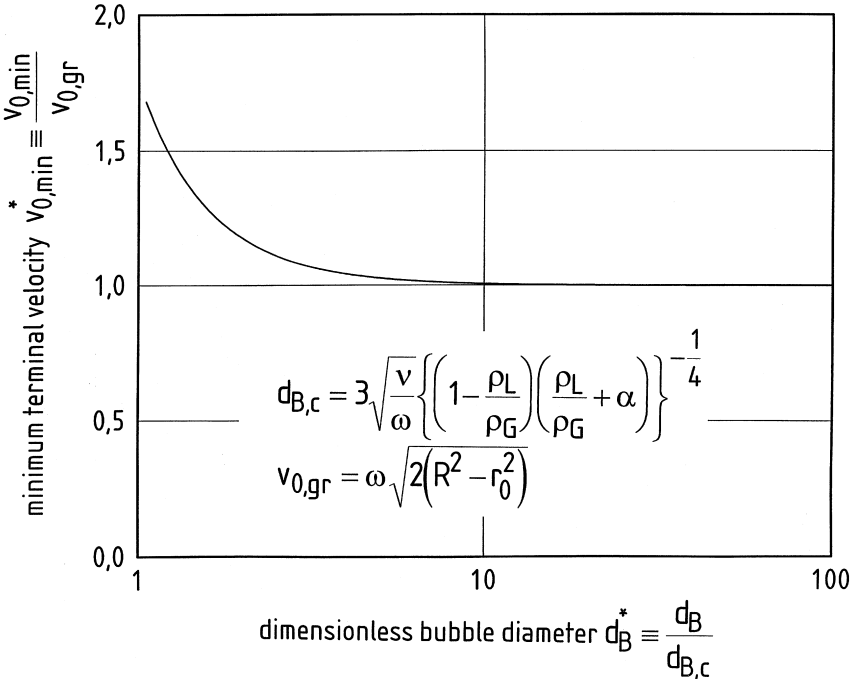

Fig. 16. Minimum terminal bubble velocity as a function of the dimensionless terminal velocity of the gas bubbles.

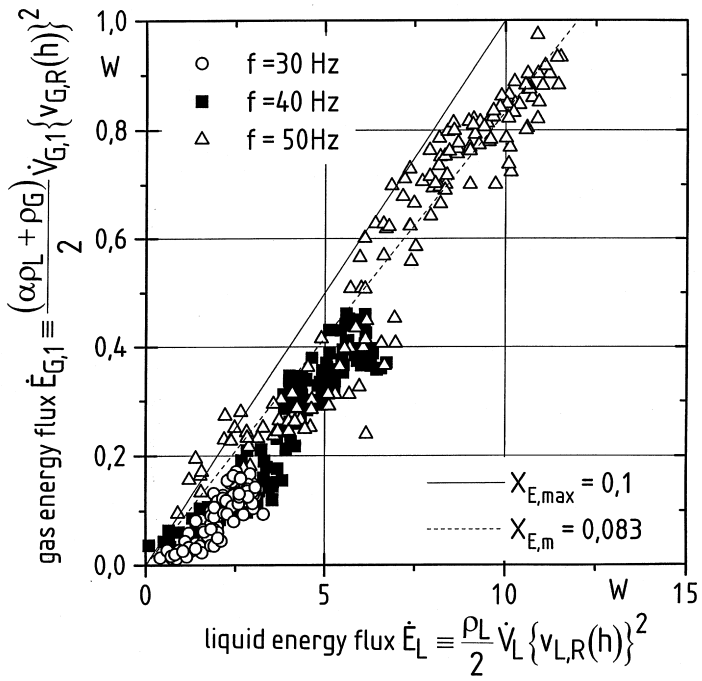

Fig. 17. Energy flux $E_{G,1}$ as a function of the energy flux E_L.

impeller is d^*_{Bl} and that the terminal velocity of these bubbles equals the minimum terminal velocity $v^*_{0,\min} = 1$ leading to

$$v_{G,R}(h) = \omega\sqrt{2(R^2 - r_0^2)}. \tag{36}$$

Experimental findings of the gas energy flux $\dot{E}_{G,1}$ are plotted versus the liquid energy flux $\dot{E}_L$ in Fig. 17 . The volumetric flow rates of gas and liquid are varied as well as the back pressure and the rotational velocity of the impeller. The gradient of the plot corresponds to the energy flux ratio. For separation frequencies $f \geq 40$ Hz the error of the model is approximately $\pm 20\%$. For small separation frequencies, the effect of friction on the trajectory of the gas bubble can not be neglected leading to a over-prediction of the energy flux $\dot{E}_{G,1}$. The energy flux ratio is assumed to characterize the geometric quality of the impeller and can technically be minimized by further optimizing the inlet section of the impeller.

7. Conclusions

A separator has been presented that enables the separation of gas and liquid for highly transient slug flows. The dynamic behavior of the separator has been modeled based on a simple physical approach without empirical factors. The theory is compared to experimental

findings. The quality of gas–liquid separation is described using a semi-empirical model. This model leads to the determination of an empirical constant that stands for the quality of the impeller. Based on a linearized theory, the scale up of the separator is enabled.

Acknowledgements

The authors gratefully acknowledge the German DFG, SFB 264 for the generous financial support.

Appendix A

A.1. Appendix A1

Linearized quantities and constants:

$$\dot{V}^{+}_{\mathrm{L1}} = \dot{V}^{*}_{\mathrm{L1}} - \dot{V}^{*}_{\mathrm{Lstat}}, \quad \dot{V}^{+}_{\mathrm{L2}} = \dot{V}^{*}_{\mathrm{L2}} - \dot{V}^{*}_{\mathrm{Lstat}}, \quad Eu^{+}_{2} = Eu^{*}_{2} - Eu^{*}_{2\mathrm{stat}}, \quad h^{+} = h^{*} - h^{*}_{\mathrm{stat}},$$

$$T_1 = \xi_{\mathrm{R}} \dot{V}^{*}_{\mathrm{stat}}, \quad T_2 = \sqrt{\frac{D^{*}_{\mathrm{R}}}{2}}, \quad T_{\mathrm{D}} = \frac{D^{*}_{\mathrm{R}}}{2\xi_{\mathrm{R}} \dot{V}^{*}_{\mathrm{stat}}} \quad K_1 = 2\xi_{\mathrm{R}} \dot{V}^{*}_{\mathrm{stat}}, \quad K_2 = \frac{\xi_{\mathrm{R}} \dot{V}^{*}_{\mathrm{stat}}}{(1 - h^{*}_{\mathrm{stat}})}. \tag{A1}$$

A.2. Appendix A2

Derivation of (Eq. (24)): The velocity of the liquid phase that reaches the interface is obtained from the momentum equation of a liquid droplet. Frictionless motion of the liquid phase is assumed. The droplet is accelerated due to the centrifugal force corresponding to the rotational velocity assuming a solid body rotation inside the impeller:

$$\frac{\mathrm{d}v}{\mathrm{d}t} = \frac{\mathrm{d}^2 r}{\mathrm{d}t^2} \approx R_{\mathrm{m}} \omega^2 \quad \forall \quad |r - R_{\mathrm{m}}| \ll R_{\mathrm{m}}. \tag{A2}$$

In this equation, v is the radial velocity of the droplet, r is the radius, R_{m} is a mean radius of the droplet motion and ω is the angular velocity. Integrating this equation two times leads to the radius of the droplet as a function of the time.

$$r = \frac{R_{\mathrm{m}}}{2} \omega^2 t^2 + R - h_{\max} \tag{A3}$$

For $t = 0$ s the radius of the droplet equals the outer radius of the inlet into the impeller $r_0 = (R - h_{\max})$. At the time $t = T$ the droplet impinges on the interface with the radius $r(t = T) = R - h$. The time T is obtained by

$$R - h = \frac{R_m}{2}\omega^2 T^2 + R - h_{max} \quad \Leftrightarrow \quad T = \sqrt{\frac{2(h_{max} - h)}{R_m \omega^2}} \tag{A4}$$

and the impinging velocity of the droplet by

$$v(t = T) = \sqrt{2R_m\omega^2(h_{max} - h)}. \tag{A5}$$

Assuming the mean arithmetic radius R_m

$$R_m \approx R - \frac{h + h_{max}}{2} \tag{A6}$$

and taking into account the definition of h^* (Eq. (8)), Eq. (41) corresponds to Eq. (24).

References

Creutz, M., 1998. Separation dreiphasiger instationär strömender Gemische. VDI Fortschritt-Berichte, VDI Verlag-Düsseldorf, Reihe 3, nr. 521, ISBN 3-18-352103-2.

Hollenberg, J.F., de Wolf, S., Meiring, W.J., 1995. A method to suppress severe slugging in flow line riser systems. 7th International Conference on Multiphase Production. 7–9. Cannes, France.

Kouba, G.E., Shoham, O., Shirazi, S., 1995. Design and performance of gas liquid cylindrical cyclone separators. 7th International Conference on Multiphase Production. 307–327. Cannes, France.

Muschelknautz, S., Mayinger, F., 1990. Strömungsuntersuchungen in der Austrittsleitung und in einem Zyklonabscheider bei Druckentlastung. Chemie-Ingenieur-Technologie 62 (7), 576–577.

Nebrensky, J.R., Morgan, G.E., Oswald, B.J., 1980. Cyclone for gas/oil separation. International Conference on Hydrocyclones. 167–178. Cambridge, UK.